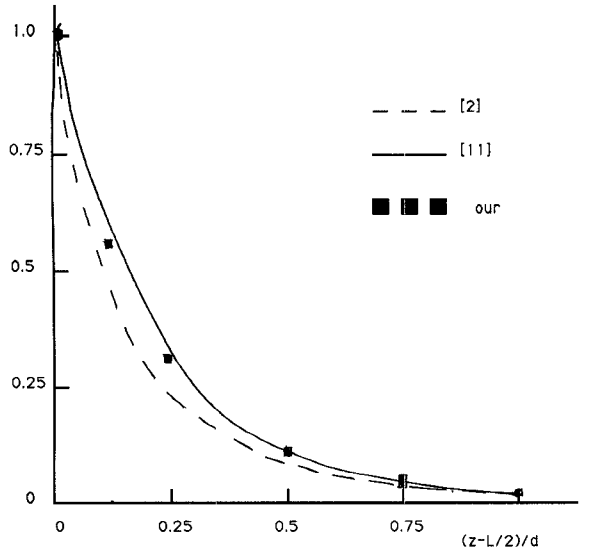


Fig. 2. The potential distribution at $x \to a_3$, $a_2 = a_1/\sqrt{1.56}$, $L/a = 1$, $\epsilon_1 = \epsilon_3 = 1$.

$$V_{3m}(\omega) = \prod_{m=1}^{M} (1 + \omega a_1/m\pi)(1 - \omega a_2/m\pi)(1 - \omega a_3/m\pi) = \prod_{m=1}^{M} \left(1 - \frac{\omega^2(a_1a_2 + a_3^2)}{(m\pi)^2} + \frac{\omega^3 a_1 a_2 a_3}{(m\pi)^3}\right). \quad (25)$$

Due to the expression

$$F(\omega) = -\frac{a_1 \sin(\omega a_2) \sin(\omega a_3)}{\omega^2 \sin(\omega a_1) a_2 a_3} \frac{A_{3M}(\omega)}{V_{3M}(\omega)} \cdot \frac{\prod_{m=1}^{M} (1 - \omega^2 a_1^2/m^2\pi^2)/(1 - \omega^2/\alpha_{m1}^2)}{\prod_{m=1}^{\infty} \left(1 + \frac{\omega^2 a_2 a_3}{m\pi(m\pi + \omega a_1)}\right) e^{-\nu\omega}}. \quad (26)$$

In the simplest case $\alpha_{n1} = n\pi/a_1$ when $\epsilon_{r1} = \epsilon_{r2} = 1$ [2] and the residue of $F(\omega)$ for $\omega = \alpha_{n1}$ is equal

$$R_F(\alpha_{n1}) = (-1)^n \frac{\sin(n\pi a_2/a_1)}{(n\pi a_2/a_3)} \frac{\sin(n\pi a_3/a_1)}{(n\pi a_3/a_1)} \frac{A_{3M}(n\pi/a_1)}{V_{3M}(n\pi/a_1)} \Big/ \prod_{m=1}^{\infty} \left(1 + \frac{n^2 a_2 a_3/a_1}{m(m+n)}\right) e^{-\nu n\pi/a_1}. \quad (27)$$

Using (27) the potential distribution is calculated and compared to the results of [2] and exact solution [11]. The coincidence is excellent with exact solution as seen from Fig. 2. Note that all results are obtained when

$$\frac{A_{3M}(n\pi/a_1)}{V_{3M}(n\pi/a_1)} = \frac{1 - (na_2/a_1)\,\mathrm{cth}\,(\pi L/(2a_2))}{1 - (na_2/a_1)} \quad (28)$$

## V. Conclusion

The described method is quite effective. It allows one to solve the problems practically in closed form and to realize all the required calculations using small computers only. The most interesting diffraction problems solved by this method are: a thick semi-infinite plate [3], infinite periodic corrugated structure [4], echelett [5] and other structures as presented in [6]–[10]. Analytical expressions for all mentioned cases were obtained.

## References

[1] R. Mittra and S. W. Lee, *Analytical Techniques in the Theory of Guide Waves*. New York: Macmillan, 1971.
[2] R. Mittra, Ed., *Computer Techniques for Electromagnetics*. New York: Pergamon 1973.
[3] V. I. Volman, Solution of the diffraction problem of the plane wave by a thick semi-infinite plate. Transactions of the Moscow Institute Radiotechnics, Electronics and Automatics, sr. AutoCAD, 1988, pp. 18–27.
[4] V. I. Volman and K. S. Daou, "Etude theorique d'un reseat infinitment conducteur par la methode de factorisation d'interpolation, *J. Optics* France, vol. 20, no. 1, pp. 35–40, 1990.
[5] V. I. Volman, "Diffraction of the plane wave by an echelett array," *Radiotechnics and Electronics* (Moscow), vol. 34, no. 4, pp. 521–527, 1988.
[6] V. I. Volman and E. Baradit, "Electrodynamic analysis of the line phase array with dielectric cover," *Radiotechnics and Electronics*, (Moscow), vol. 35, no. 12, pp. 2484–2491, 1989.
[7] V. I. Volman and A. Volosskij, "Diffraction of plane wave by a strip grating," *Orjenickidze*, 1989.
[8] V. I. Volman, K. U. Pimenov, "Electrodynamic analysis of step waveguide connection of rectangular waveguide," *Trans. NIIR* (Moscow), no. 2, pp. 111–116, 1989.
[9] V. I. Volman and M. A. Mamchin, "Analytical method of electrodynamic analysis of the step connection of two coaxial lines," *Radiotechnika* (Moscow), no. 4, pp. 65–68, 1988.
[10] ——, "Results of the exact analysis of a step connection of coaxial lines with several cross-sectional form and dielectric filling," Collection, *Electrodynamic System and Deviçes* (Saratov), pp. 4–10, 1989.
[11] V. Volman, Ed., "Calculation and design of microwave strip line devices handbook," *Radio and Telecommunication*, USSR, 1982.

# Optimal Microwave Source Distributions for Heating Off-Center Tumors in Spheres of High Water Content Tissue

Carey M. Rappaport and Jorge G. Pereira

***Abstract*—A surface distribution of electric dipoles can be used to represent a multi-element microwave hyperthermia applicator for non-invasive heating of off-center targets within a spherical high-water-content tissue volume—such as the head. This paper presents a method for finding the optimal surface distributions for delivering maximum power for arbitrarily located deep tumors in such a uniform spherical volume. The resulting focused power dissipation pattern for any tumor location has a global maximum at the tumor, and also is the largest spherical volume for which no healthy tissue is overheated. The optimization uses spherical field harmonics, centered at the tumor target, summed with suitable complex weights to iteratively minimize surface power. Once the best field distributions are derived, the current sources which generate these distributions are determined. The resulting excitations represent the theoretically ideal spherical microwave hyperthermia configuration for which no physical applicator system can surpass.**

## Introduction

A major advantage of electromagnetic hyperthermia is the ability to control constructive and destructive interference in locations removed from the antenna applicator. Ideally, focusing power on a

Manuscript received October 1, 1991; revised March 17, 1992.
The authors are with the Center for Electromagnetics Research, 235 Forsyth Building, Northeastern University, Boston, MA 02115.
IEEE Log Number 9202147.

deep tumor selectively heats it to temperatures high enough to kill cancerous cells without overheating and harming surrounding healthy tissue.

This work extends the analytical framework used to study field focusing within a high-water-content biological tissue volume. Other studies of explicitly focused electromagnetic sources suggest means to increase power density at a deep focal point [1]–[3], but not to above surface levels—and hence do not present a therapeutically beneficial heating scheme. A practical electromagnetic applicator must have a three-dimensional global maximum at the tumor.

In previously reported studies [4], [5], the optimal field distribution for heating a tumor at the *center* of a biological sphere was derived. These studies present the spherical optimization method of using higher order spherical modes—which have zero field in the center—to cancel the first order mode field maxima on the sphere's surface. The first order completely determines the field at the center, while these higher order modes destructively interfere to make the field at the surface almost uniform. Thus, for a given radius sphere, the volume field distribution with the greatest ratio of target field to surface field can be found. The sphere radius is then increased and optimization repeated until the field amplitudes of the target almost equals those of the surface. This radius represents the largest spherical volume with a global power maximum at its center, and hence the deepest tumor which can be electromagnetically heated safely and efficiently.

It is also shown in these previous studies that 915 MHz is the best standard (ISM) frequency for deep heating with appreciable resolution. The maximum sphere radius at 915 MHz is 9.45 cm. For higher frequencies the deposited power pattern resolution at the target is greater—and the attenuation-to-propagation ratio is smaller—but since the attenuation is exponential, while the illuminating aperture grows only quadrically with aperture area, the shorter wavelength limits the maximum sphere radius. For much lower frequencies (i.e. 100 MHz) the largest sphere is larger than for 915 MHz, but the smaller electrical aperture leads to less constructive interference, with poorly resolved focal spots. At such low frequencies, focusing makes very little difference on the power pattern.

A similar iterative, two-step field shaping technique is used in this study for a non-symmetrical geometry, with a tumor centered (without loss of generality) at an eccentric target point on the polar axis. The optimal total field inside the irradiated sphere of muscle tissue is then parameterized in terms of complex modal coefficients which can be used to specify a surface current and dipole distribution. The present study finds the z-polarized focal field maximum in terms of a polar source distribution function.

An alternative, orthogonal polarized focal field can be derived in terms of just the azimuthal modes (each of which is orthogonal to the polar modes). However, the field distribution for either polarization is dominated by the radial dependence of the spherical Bessel functions, with higher order modes canceling the fundamental focal mode in similar ways. The azimuthal optimum focused field has almost the same maximum radius. It will be described in a subsequent paper.

## Principles of Modal Field Optimization

We consider a sphere of uniform biological tissue which is centered at the origin of a primary rectangular coordinate system and excited at 915 MHz. Muscle tissue, which is used as the typical high-water-content biological medium, has measured wave number [6] $\kappa = (2\pi/\lambda)(1 - j0.23)$, and wavelength $\lambda = 4.5$ cm. It is assumed that the focal target is on the z-axis, at some fraction of the sphere radius from its center. Using the same principle as for the centered target, the electric field is written as a sum of spherical harmonics. In this eccentric case however, in order to isolate a single mode as the only non-zero contribution to power at the target, the harmonics must be specified in terms of auxiliary translated coordinates, centered at the target. This geometry, with auxiliary frame of reference identified with primed coordinates is shown in Fig. 1.

Taking into account the azimuthal symmetry of this heating problem, the electric field is given by:

$$\vec{E}(\vec{r}) = \sum_{n=1}^{\infty} \hat{r}B_n \frac{n(n+1)}{\kappa r'} j_n(\kappa r')P_n(\cos\theta') + \hat{\theta}B_n\left[ j_{n-1}(\kappa r') - \frac{n}{\kappa r'} j_n(\kappa r')\right] \times [n\cos\theta' P_n(\cos\theta') - nP_{n-1}(\cos\theta')] \frac{1}{\sin\theta'} \quad (1)$$

where $P_n$ and $j_n$ are the *nth* order Legendre and Bessel functions, respectively, and $B_n$ are the *nth* complex weighting coefficients. Equation (1) indicates that for surface field points where the radial coordinate is large, the $\theta$ component contribution to deposited power (proportional to $|\vec{E}|^2$) is dominant. Also, using the asymptotic approximation for the spherical Bessel function for small radial arguments, $j_n(\kappa r) \sim (\kappa r)^n/1 \cdot 3 \cdot 5 \cdots (2n+1)$, to evaluate the electric field at the focus $r' = 0$, gives $|\vec{E}(\vec{r})|_{r'=0} = 2/3\, B_1$, with contribution from only the first mode. Fig. 2 shows the amplitude of the first mode ($n = 1$) of the electric field in a cross section through the poles of the sphere for a target at $z = 0.6R$, $R = 7.7$ cm. Note that the field maximum occurs at the eccentric target, and that the highest field levels are on the sphere surface farthest from the target.

Appropriate higher order modes, $n = 2, 3, 4, \cdots$, can now be added to the first mode to reduce the harmful single mode surface field without altering the field value at the hot spot tumor target. In the secondary frame of reference $E_\theta$ of (1) is separated into the product of a polar dependent part and a radially dependent part, given by $C_n = B_n[j_{n-1}(\kappa r') - (n/\kappa r')j_n(\kappa r')]$. Since $\kappa$ is complex, $C_n$ is complex; its phase solely determines the phase of $E_\theta$. On the surface of the tissue sphere ($r = R$) the relationship between secondary coordinate radius and primary polar angle can be cast in terms of the target point $f$, as

$$r'(\theta) = -f\cos\theta + \sqrt{f^2\cos^2\theta - f^2 + R^2}. \quad (2)$$

The field synthesis involves $N$ higher order modes with coefficients $B_n$, and $2N$ real optimization variables. However, if the phase variation of each mode coefficient is similar to that of the first mode, only the mode *amplitudes* would need to be adjusted. Choosing the constant phase offset for each mode which sets all modal fields to be purely real and positive at the polar angle where the first mode amplitude peaks, yields the modal phase variations shown in Fig. 3 for the $f = 0.6R$ case. In the vicinity of the polar coordinate $\theta = \theta_0 = 0.64\pi$, the phases of all the modes are almost independent of mode order (except for the constant offset). The phase difference between the modes is not insignificant for polar locations far from the zero-phase polar angle, however Fig. 1 indicates that the amplitude of the first mode distribution at these angles is much smaller than at the zero-phase angle. Since the algorithm is designed to lower field levels below a given threshold level, the high phase differences shown in Fig. 3 does not compromise the efficiency of the algorithm.

Writing the $\hat{\theta}$-component of each mode of (1) in magnitude/phase form, $E_{\theta n} = |B_n|e^{j(\Phi_1(\theta_0') - \Phi_n(\theta_0'))}M_n(\theta')e^{j\Phi_n(\theta')}$ yields total field mag-

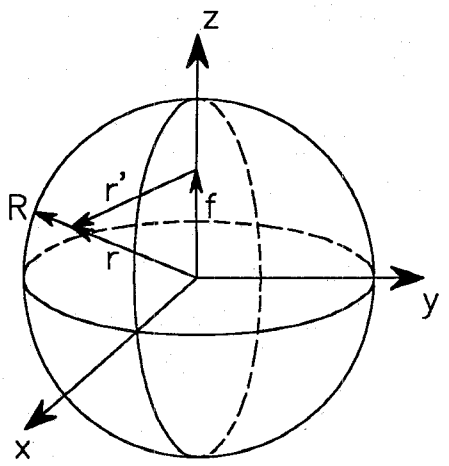


Fig. 1. Spherical eccentric field focusing geometry.

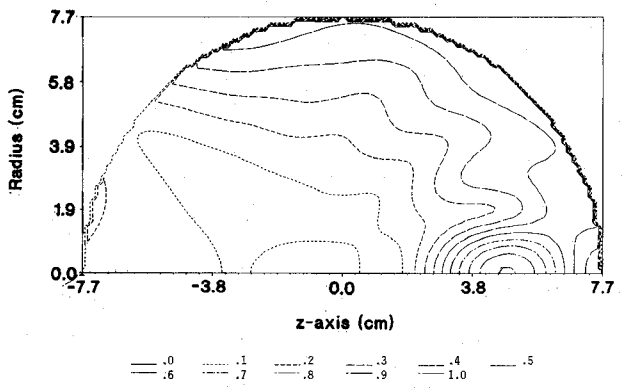


(a)

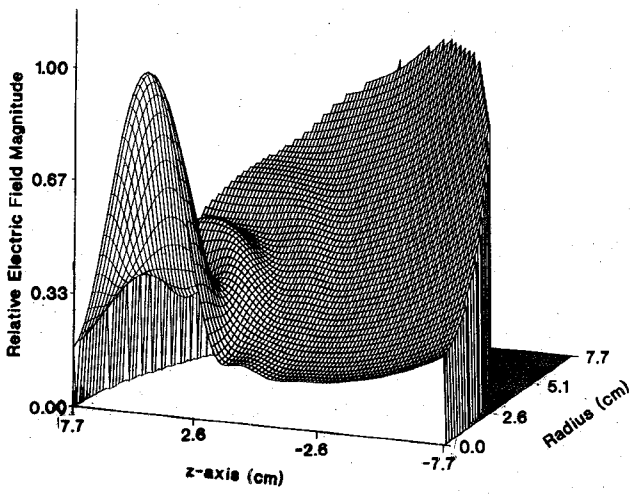


(b)

Fig. 2. E-field intensity of the first off-center spherical harmonic, centered at $z = 0.6R$, as a function of position $(\rho, z)$. (a) Contour plot. (b) Surface plot.

nitude:

$$|E_{\text{tot}}| \approx \|B_1|M_1(\theta') + \sum_{n=2}^{N} |B_n|M_n(\theta') \exp\,[j(\Phi_n(\theta') - \Phi_n(\theta_0') - (\Phi_1(\theta') - \Phi_1(\theta_0')))]|.$$

Near the first mode surface power peak, $\theta' = \theta_0'$, $r = R$, $\Phi_n(\theta') - \Phi_n(\theta_0') \approx (\Phi_1(\theta') - \Phi_1(\theta_0'))$, implying that the phase-shifted higher order modes have very little phase dependence on polar angle, and the optimization proceeds assuming they are purely real. As such,

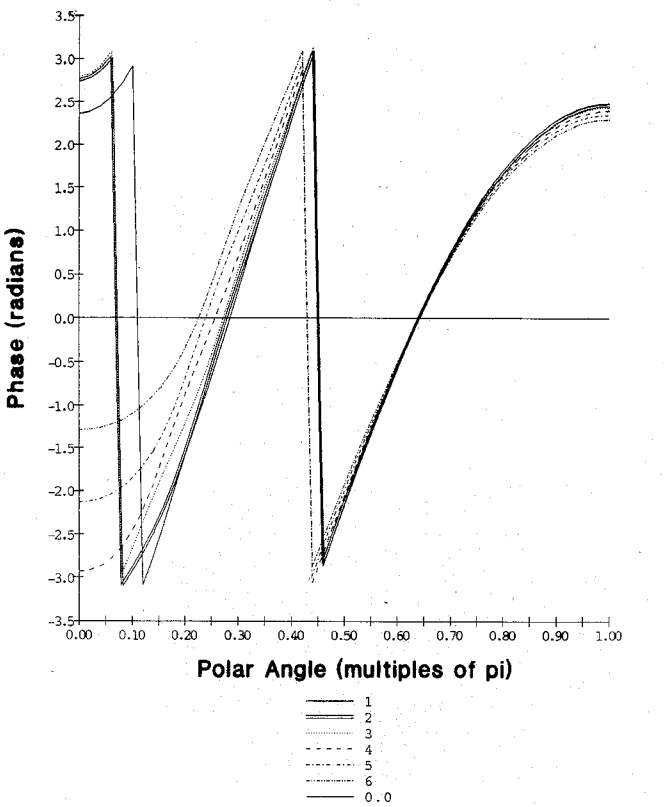


Fig. 3. Phase as a function of polar angle for each of the first 6 modes, with the phase at $\theta = .64\pi$ subtracted.

the optimization is linear with respect to $|B_n|$ and only $N - 1$ variables need be found. The reduction is implemented by the politope method [7], using a computer routine [8] which minimizes the area defined by the surface field curve above a given threshold setting.

After several iterations of extending the sphere radius $R$ and then suppressing surface power levels to that of the focal point, the following optimal six-mode ensemble was found which heat the target tumor at $0.6R$ in a high water content, 12-cm radius sphere with relatively uniform surface fields: $B_n = 1.5e^{j2.158}$, $0.834e^{j0.326}$, $0.288e^{j1.598}$, $0.132e^{j2.726}$, $0.105e^{j0.53}$, $0.071e^{j1.473}$. These excitation coefficients constitute an optimum since at the 12-cm radius no additional higher order modes could be added to appreciably lower the surface power. The optimized field profile for the sphere half cross-section is presented in Fig. 4. Harmonic translation formulations given in [8] can be employed to cast the optimal modal coefficients in the primary frame of reference as follows:

$$\vec{E}(\vec{r}) = \sum_{n=1}^{\infty} A_n^- [\hat{r}E_{rn}(r, \theta) + \hat{\theta}E_{\theta n}(r, \theta)] \tag{3}$$

where $E_{rn}$ and $E_{\theta n}$ are similar to (1), and the first six coefficients are: $A_n^- = 1.187e^{j2.675}$, $1.295e^{j2.445}$, $0.7134e^{j2.293}$, $0.416e^{j2.143}$, $0.356e^{j1.839}$, $0.238e^{j1.671}$.

## Specification of the Surface Distribution

The applicator current sources which generate the required field distribution as closely as possible are now derived. This distribution can be modeled as a charge double layer (which yields a discontinuous tangential component of the electric field) and the usual surface current. The symmetry of the problem suggests that the source distribution is independent of $\phi$ and has no $\phi$ component. Thus, the current source can be given as:

$$\vec{J} = \sum_{n=1}^{N} [\hat{r}F_{rn}(\theta) + \hat{\theta}F_{\theta n}(\theta)]\delta(r - R) \tag{4}$$

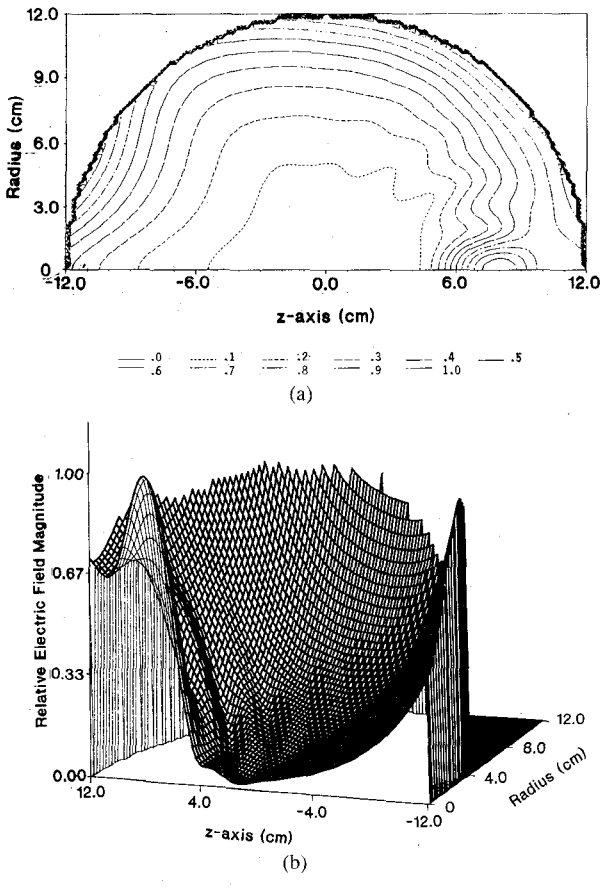


Fig. 4. Optimal multi-mode E-field profile for focal target at $0.6R_{\max}$, $R_{\max}$ = 12.0 cm. (a) Contour plot. (b) Surface plot.

where $N$ is the total number of modes and $R$ is the constant radius of the sphere of muscle tissue. The functions $F_{rn}(\theta)$ and $F_{\theta n}(\theta)$ in (4) are determined from application of the boundary conditions at the surface of the sphere [9]. Using the formula for charge continuity $\nabla \cdot \vec{J} = -j\omega\rho$ gives the charge at the spherical surface:

$$\sigma_s = \frac{2F_{rn} + \dfrac{dF_{\theta n}}{d\theta} + F_{\theta n} \cot\theta}{r} \tag{5}$$

and

$$p_\Sigma = \frac{1}{j\omega} F_{rn} \tag{6}$$

and $\rho = \sigma_s\delta(r - R) - p_\Sigma\delta'(r - R)$ and singularities have been matched. Here $\sigma_s$ is the surface charge and $p_\Sigma$ is the double layer amplitude.

The $E$-fields inside the sphere are given by (3). The $H$-fields have the form:

$$\vec{H} = -\hat{\phi}\frac{jA_n^-}{\eta^-} j_n(\kappa^- r)\frac{dP_n(\cos\theta)}{d\theta}. \tag{7}$$

The fields outside have the same form with the spherical Bessel functions $j_n(\kappa^- r)$ replaced by the outgoing spherical Hankel function $h_n^{(2)}(\kappa^+ r)$ (assuming $e^{j\omega t}$ time dependence). The modal coefficients $A_n^-$ and $A_n^+$ as well as the wave numbers $\kappa^-$, $\kappa^+$ and impedances $\eta^-$, $\eta^+$ indicate modes inside and outside the sphere, respectively.

Two boundary conditions at the sphere surface are needed to specify $A_n^+$ in terms of the $A_n^-$ given in (3). Ampere's Law gives the tangential $H$-field condition, which using (4) and (7) gives

$$F_{\theta n} = -j\frac{dP_n(\cos\theta)}{d\theta}\left[A_n^- \frac{j_n(\kappa^- R)}{\eta^-} - A_n^+ \frac{h_n^{(2)}(\kappa^+ R)}{\eta^+}\right]. \tag{8}$$

The differential form of Gauss's Law with the double-layer singularity is multiplied by $r - r'$ and integrated from $r^-$ to $r^+$ and across a differential element of surface area, and then converted to scalar and vector potential form and eventually gives the tangential $E$-field condition [10] in terms of the surface gradient of the double layer amplitude: $\epsilon^+\vec{E}_\theta^+ - \epsilon^-\vec{E}_\theta^- = -\nabla_\Sigma p_\Sigma$. Integrating with respect to $\theta$ using (3) and (6) gives

$$F_{rn} = jP_n(\cos\theta)\frac{d}{dr}\left[A_n^- \frac{rj_n(\kappa^- r)}{\eta^-} - A_n^+ \frac{rh_n^{(2)}(\kappa^+ r)}{\eta^+}\right]\Bigg|_{r=R}. \tag{9}$$

Now (8) and (9) are substituted into the differential equation (5), and since it is assumed that there are no perfect conductors in the given geometry, there is no net surface charge, $\sigma_s = 0$. The resulting equation uses a Legendre function recurrence relation [11] to eliminate the $\theta$ dependence. Solving for the remaining unknown results in

$$A_n^+ = A_n^- \frac{\eta^+}{\eta^-}\frac{n(n-1)j_n(\kappa^- R) + 2\kappa^- R j_{n-1}(\kappa^- R)}{n(n-1)h_n^{(2)}(\kappa^+ R) + 2\kappa^+ R h_{n-1}^{(2)}(\kappa^+ R)} \tag{12}$$

Each individual modal oscillation is associated with its own surface source distribution which follows from (4) using (8) and (9) with everything specified in terms of $A_n^-$ given in (3). The equivalent current density representing the applicator can be modeled as the superposition of all individual modal source distributions.

It must be emphasized that this optimization procedure provides a theoretical limit for deep heating. In practice, no actual applicator would be able to generate as good a power pattern. We have presented instead a "benchmark" for judging electromagnetic hyperthermia feasibility. Just as with thermodynamic efficiency cycles, knowledge of ideal heating limits provides essential information for designing practical medical treatment devices.

## References

[1] J. Loane, H. Ling, B. Wang, and S. Lee, "Experimental investigation of a retro-focusing microwave hyperthermia applicator: conjugate field matching scheme," *IEEE Trans. Microwave Theory Tech.*, vol. MTT-34, no. 5, May 1986, pp. 490–493.

[2] W. Gee, S. Lee, N. Bong, C. Cain, R. Mittra, and R. Magin, "Focused array hyperthermia applicator: theory and experiment," *IEEE Trans. Biomed. Eng.*, vol. BME-31, no. 1, Jan. 1984, pp. 38–46.

[3] S. Wright and R. Magin, "Analysis of planar microstrip arrays for microwave hyperthermia," in *1991 PIERS Symp.*, July 1991, p. 111.

[4] C. Rappaport and F. Morgenthaler, "Optimal source distribution for hyperthermia at the center of a sphere of muscle tissue," *IEEE Microwave Tech.*, vol. MTT-35, no. 12, Dec. 1987, pp. 1322–1327.

[5] ——, *Synthesis of Optimum Microwave Antenna Applicators for Use in Treating Deep Localized Tumors*, in *PIERS* series, J. A. Kong, Ed. New York: Elsevier, 1988.

[6] C. Johnson and A. Guy, "Non-ionizing electromagnetic wave effects in biological materials and systems," *Proc. IEEE*, vol. 60, no. 6, June 1972, pp. 692–718.

[7] P. Gill, W. Murray, and M. Wright, *Practical Optimization.* New York: Academic Press, 1981.

[8] J. Pereira, *Double Layer Ideal Spherical Model of an Optimal Microwave Power Transducer*, M.S. thesis, Dept. of Elec. Comp. Eng., Northeastern University, Boston, 1990.

[9] C. Rappaport, "Comments on 'synthesis of optimum microwave antenna applicators for use in treating deep localized tumors' by C. M. Rappaport, *PIER 1*, 1989," in *J. Elect. Waves Appl.*, vol. 5, no. 3, July 1991.

[10] J. Melcher, *Continuum Electromechanics.* Cambridge: MIT Press, 1981, p. 2.16.

[11] M. Abramowitz and I. A. Stegun, *Handbook of Mathematical Functions*, NBS Applied Math Series 55, Dec. 1972.